Petroleum Science 19 (2022) 354–362

Contents lists available at ScienceDirect

Petroleum Science

journal homepage: www.keaipublishing.com/en/journals/petroleum-science

Original Paper

# The role and potential of attapulgite in catalytic pyrolysis of refinery waste activated sludge

Qinghong Wang [a], Kanghong Hao [a], Chelsea Benally [b], Yue Kou [a], Zhexuan An [b], Mohamed Gamal El-Din [b], Chunmao Chen [a, *]

[a] State Key Laboratory of Heavy Oil Processing, Beijing Key Laboratory of Oil and Gas Pollution Control, China University of Petroleum-Beijing, Beijing, 102249, China
[b] Department of Civil and Environmental Engineering, University of Alberta, Edmonton, Alberta, T6G 1H9, Canada

ARTICLE INFO

*Article history:*
Received 27 November 2020
Accepted 7 June 2021
Available online 2 October 2021

Edited by Xiu-Qiu Peng

*Keywords:*
Catalytic pyrolysis
Attapulgite
Kinetics
Product characteristics

ABSTRACT

Pyrolysis is a promising technology for the treatment of refinery waste activated sludge (rWAS). In this study, attapulgite as a natural clay was used to enhance the pyrolysis of rWAS. The yields, characteristics of pyrolytic products, pyrolytic kinetics and mechanisms were investigated. The attapulgite improved the conversion of rWAS into non-condensable gases and pyrolytic liquids. The bio-oil quality improved and the biochar yield reduced. The average activation energy of Stage I (230–400 °C) and Stage II (400–500 °C) decreased by 36.5% and 49.7%, respectively, compared to rWAS alone. $Al_2O_3$ and $Fe_2O_3$ in attapulgite enhanced the dealkylation reaction and cracking of C–C bonds. The content of the gasoline (<$C_{13}$) fraction of bio-oil doubled relative to rWAS alone. Attapulgite promoted the deoxygenation, dehydroxylation and dehydrogenation reactions of O-containing compounds, and the content of CO and $CO_2$ in non-condensable gases increased. Addition of attapulgite (rWAS:attapulgite ratio of 1:1) decreased the O mobility from 14.6% to 12.8% relative to rWAS alone. Also, the content of saturates in bio-oil increased from 38.5 wt% to 47.2 wt% and the lower heating value (LHV) increased from 6.8 kcal/kg to 8.4 kcal/kg. The heavy metals originally in rWAS were fixed into the pyrolytic residue and the environmental risks are low. This study demonstrates the role and potential of attapulgite in catalytic pyrolysis of rWAS with an added advantage of increased cost-effectiveness.


## 1. Introduction

A great amount of refinery waste activated sludge (rWAS) is generated from biological treatment processes in refinery wastewater treatment plants (WWTPs). rWAS is mainly biomass but also contain high contents of organic contaminants, heavy metals and inorganic impurities. Conventional methods of disposal for rWAS usually includes landfill disposal, composting, anaerobic digestion, and incineration (Liu et al., 2009; Yang et al., 2015). Landfills are a final disposal method for many hazardous wastes, however this method is not preferred due to the associated environmental risks that can result from the leakage of hazardous chemicals into the vadose zone and the underlying aquifer (Mishra et al., 2017). Composting can convert the nitrogen, phosphorus, and organic matters in biological sludge to nutrients and humus for agricultural uses (Raheem et al., 2018). However, the high content of heavy metals and oils in rWAS hinders the use of composting. Anaerobic digestion is effective in the recovery of value-added energies (e.g. $CH_4$ and $H_2$) from biological sludge. However, the poisonous and harmful substances in rWAS often inhibit digestion efficiency and reduce the production of energies (Nges and Liu, 2010). Lastly, incineration can completely decompose the rWAS. The energy from organic matters can only partially supplement the required heat for incineration. As a result, secondary treatment for hazardous residual ash and flue gas are often needed post incineration (Gong et al., 2018).

Pyrolysis is a thermal-chemical process that can convert organic matter in sludge into gaseous, liquid and solid products in an inert environment. Pyrolysis exhibits great potential in rWAS treatment with the advantages of sludge reduction, production of value-added energies, as well as immobilization of hazardous chemicals

* Corresponding author.
*E-mail address:* c.chen@cup.edu.cn (C. Chen).

https://doi.org/10.1016/j.petsci.2021.09.043

(Fonts et al., 2012). Pyrolysis conditions and properties of sludge are related to the pyrolysis mechanisms and characteristics of products. During municipal sludge pyrolysis, an increase of termination temperature can dramatically reduce the residue yield while significantly increasing the total yields of bio-oil and gases (Zhou et al., 2019). At 850 °C, the highest conversion for municipal sludge was obtained and 74% of energy was recovered by pyrolytic syngas and tar (Karaca et al., 2018). Furthermore, high termination temperature may decrease the ratio of bio-oil to syngas, and promote the dehydrogenation and polymerization reactions of short-chain hydrocarbons, enhancing the generation of $H_2$, aromatic and polyaromatic compounds (Lin et al., 2019). Thus, the $H_2$ content in pyrolytic gases and aromatics in bio-oil both increase. The high temperature also promotes the gasification of residue and decomposition of primary vapor, increasing the production of pyrolytic gases as well as the content of $H_2$, CO and $CH_4$ (Shen and Yoshikawa, 2013; Han et al., 2015).

Introduction of catalysts into the sludge pyrolysis can greatly accelerate the reactions as well as improve yields and qualities of pyrolysis products. A variety of catalysts, such as metallic oxides, natural minerals, zeolites and even solid wastes, have been used in sludge pyrolysis (Shao et al., 2010; Zhao et al., 2013). γ-$Al_2O_3$ may promote the aromatization reaction and then facilitate the formation of aromatic and polycyclic compounds. γ-$Al_2O_3$ also assists the deoxygenation reaction of fatty acids, upgrading the quality of the organic phases which affect the resulting LHV, viscosity, steadiness, and chemical composition (Azuara et al., 2015). Dolomite can promote the conversion of aromatics and heavy hydrocarbons into light aliphatic hydrocarbons (Lin et al., 2019). The catalytic cracking performance of natural minerals can be enhanced by loading metal oxides such as Fe, Mg, Ni, etc. Mg-supported natural aluminosilicate clay removes 94% of alkanes from the pyrolytic gases (Zabłocka-Malicka et al., 2016). Fe/Ni-based palygorskite enhances the cracking reaction of tar vapor and more gaseous products ($H_2$ and $CH_4$) (Liu et al., 2010). The attapulgite, with a hydrated Mg–Al–Si crystal, has an exceptionally low market price due to earth-abundant reserve (Cui et al., 2013). The potential use of attapulgite or metals loaded attapulgite in catalytic pyrolysis of organic matters and biomass has been previously demonstrated (Li et al., 2015). To our knowledge, it has not been utilized as a catalyst during the pyrolysis treatment of rWAS.

This study aims to: (1) investigate the effect of natural attapulgite as a catalyst to pyrolyze rWAS, (2) characterize the pyrolytic products and determine the pyrolytic products yields, (3) investigate the rWAS pyrolysis mechanisms involved with attapulgite catalytic.

## 2. Materials and methods

### 2.1. Materials preparation

The rWAS was obtained from the WWTP in the Liaohe Petrochemical Company of China. Attapulgite was purchased from Gansu Haodi Mining Co., Ltd. Both of the rWAS and attapulgite were dried for 24 h at 105 °C to remove the moisture before use and sieved into fine particles (<75 μm). However, 9 wt% of bound water were still in the attapulgite.

### 2.2. Pyrolysis experiments

In each experiment, attapulgite with a designed ratio (rWAS: attapulgite = 1:0, 1:0.5, 1:0.75 and 1:1) was mixed with 20 g of rWAS and then put into the pyrolysis reactor. The reactor was heated by a STGK-100-12 horizontal tube furnace (SanTe, Luoyang, China). During the pyrolysis process, $N_2$ (1 L/min) was used to purge air to ensure there was an inert environment. Then heating each sample to 650, 750 and 850 °C for 60 min with an uninterrupted rate of 0.5 °C/s, respectively. And the pyrolytic vapors were condensed to collect the liquid products including bio-oil and water. The non-condensable gases were collected in collection bags. Pyrolytic residue was taken out from the pyrolysis reactor not until cooling to the room temperature. Each experiment was performed in duplicate.

### 2.3. The calculation of pyrolytic products yields

At a high temperature, the bound water will separate from the attapulgite and amplify the yield of pyrolytic liquids. The actual yields of pyrolytic gases, liquids and residue are related to rWAS in this study. Therefore, the influence of the bound water in attapulgite on yield of pyrolytic liquids should be eliminated. The pyrolytic residue ($M_T$, g) include the attapulgite added ($M_A$, g) and the biochar ($M_{Bc}$, g) from rWAS. The yield of biochar ($C_{Bc}$, 100%) and liquid ($C_L$, 100%) were defined as the ratio of biochar ($M_{Bc}$, g) to rWAS ($M_S$, g) (Formula 1), and pyrolytic liquid ($M_L$, g) to rWAS ($M_S$, g) (Formula 2), respectively. Then the non-condensable gases yield ($C_G$, 100%) was calculated by Formula 3. The reduction rate ($C_R$, 100%) of rWAS was calculated by Formula 4.

$$CBc = \frac{M_{Bc}}{M_S} \times 100\% = \frac{M_T - 0.91 \times M_A}{M_S} \times 100\% \quad (1)$$

$$C_L = \frac{M_L - 0.09 \times M_A}{M_S} \times 100\% \quad (2)$$

$$C_G = 100\% - C_{Bc} - C_L \quad (3)$$

$$C_R = 100\% - C_{Bc} \quad (4)$$

### 2.4. Characterization and analysis

#### 2.4.1. Analysis of attapulgite and rWAS

The elemental contents of rWAS and bio-oil were measured by an elemental analyzer (Vario EL III, Elementar Analysen Systeme GmbH, Germany). Proximate analysis of rWAS was carried out according to Test method No. E871, E872 and D1102 of ASTM standard, and the fixed carbon content in rWAS was calculated according to Liu et al. (2015). The oil content of pyrolytic residue and raw rWAS were determined according to the HJ 637–2018 standard. XRF Spectrometer (Panalytical BV, Almelo, Netherland) was used for determination of metal compositions of attapulgite and rWAS.

#### 2.4.2. Analysis of bio-oil

Bio-oil was separated from the pyrolytic liquids after settlement. The organic compositions were analyzed by an Agilent 7890B-5977A GC-MS spectrometer (Agilent, Palo Alto, America) according to Ye et al. (2020). The saturates, aromatics, resins and asphaltenes (SARA) fractions were measured according to the standard method of SY/T 5119-2008 (Lin et al., 2017) using an AcceleSep accelerated separation system (Agela, Tianjin, China). The lower heating values (LHV) were measured by a calorific analyzer (HY-A9, HENGYA, China) using the ASTM bomb calorimeter method. The mobility ($M$) of O element was defined as follows (Cheng et al., 2017).

$$M = \frac{Wo}{Ws} \times 100\% \quad (5)$$

where $W_s$ represents the weight percentage of O in the rWAS, and $W_o$ is the weight percentage of O in the bio-oil.

#### 2.4.3. Analysis of non-condensable gases

An Agilent 6890A gas chromatograph (Agilent Palo Alto, America) was used to analyze the collected non-condensable gases. LHV calculation of the gas followed formula (6) (Gil-Lalaguna et al., 2014):

$$LHV_{gas} = \sum_{i=1}^{n} C_i \times LHV_i \quad (6)$$

where $C_i$ and $LHV_i$ are the molar percentages and lower calorific values of CO, $H_2$, $CH_4$, and $C_2H_n$, respectively, $LHV_{gas}$ is the lower heating value of the gases.

#### 2.4.4. Characterizations of pyrolytic residue

Pyrolytic residue includes the biochar from the rWAS and the added attapulgite. The surface functional groups were investigated by a FT-IR spectrometer (Magna-IR 560 ESP, Nicolet, America). Heavy metals in pyrolytic residues were extracted according to Xu et al. (2017) using Tessier's method, and then measured by an ICP-OES (OPTIMA 7300V, Perkin Elmer, America). *LHV* of pyrolytic residues were measured using an HY-A9 calorific meter.

### 2.5. Thermogravimetric analysis and kinetics

The rWAS samples were analyzed by thermogravimetric (TG) and derivative TG (DTG) using a thermal analyzer (STA449 F3, Netzsch, Germany). Total weight of 10 mg mixture in the ratios of rWAS with attapulgite as 1:1, 1:0.75, 1:0.5 and 1:0 were heated to 900 °C in a nitrogen environment. The pre-exponential factor ($A$), activation energy ($E$) and kinetic parameters of pyrolysis process were investigated according to the DTG curves using the Coats–Redfern method. And the Coats-Redfern equations followed formula (7) and (8) (Gao et al., 2014):

$$ln\left[\frac{1-(1-\alpha)^{1-n}}{T^2(1-n)}\right] = ln\left[\frac{AR}{\beta E}\left(1-\frac{2RT}{E}\right)\right] - \frac{E}{RT}, \ n \neq 1 \quad (7)$$

$$ln\left[\frac{-ln(1-\alpha)}{T^2}\right] = ln\left[\frac{AR}{\beta E}\left(1-\frac{2RT}{E}\right)\right] - \frac{E}{RT}, \ n = 1 \quad (8)$$

where $\alpha$ is the conversion rate of rWAS, $\alpha=(m_0-m_i)/(m_0-m_f)$, where $m_0$, $m_i$, and $m_f$ indicate the initial, present, and final residual mass of samples, respectively. R is the universal gas constant (R = 1.986 cal/(mol•K)); $T$ is the temperature, K; and $\beta$ is the constant heating rate, K/min.

Plots of $\ln[(1-(1-\alpha)^{1-n})/(T^2(1-n))]$ *versus* $1/T$ for samples were graphed. $A$ and $E$ values were calculated based on the intercept and slope in the Arrhenius plot at each experimental data with different ratios of rWAS to attapulgite.

## 3. Results and discussion

### 3.1. Properties and compositions of rWAS and attapulgite

The rWAS has high contents of ash (32.9 wt%), fixed carbon (11.4 wt%) and volatile (49.2 wt%) (Table S1). The rWAS showed a high oil content (7.0 wt%), as well as high C (37.6 wt%), H (5.4 wt%), S (2.6 wt%) and O (17.4 wt%) contents in comparison with sewage sludge (C = 17.7 wt%, O = 13.1 wt%, H = 3.2 wt% and S = 0.4 wt%) (Hu et al., 2018). The high content of organic matter in rWAS benefits the generation of value-added pyrolytic product (such as oils and gases). The ash in rWAS is mainly $SiO_2$, $Al_2O_3$, $Fe_2O_3$, CaO, and $Na_2O$ (Table S2). The ash may catalyze the pyrolysis (Cheng et al., 2017). The main chemical compositions of attapulgite were $SiO_2$, $Al_2O_3$, MgO, $Fe_2O_3$, CaO and $K_2O$.

### 3.2. Pyrolytic products yields

The increase of termination temperature promoted the pyrolytic gas yield (Fig. 1), which increased from 16.1 wt% to 19.7 wt% with the termination temperature raised from 650 °C to 850 °C for the pyrolysis of rWAS alone. The increased yield of pyrolytic gas at high temperatures is mainly attributed to the secondary cracking of pyrolytic vapors (Syed-Hassan et al., 2017). Metallic oxides in rWAS, which consist of $Al_2O_3$, MgO, $Fe_2O_3$, CaO, ZnO, $Na_2O$, $K_2O$ and so on, may favor the cracking of pyrolytic vapors (Shen et al., 2016). High temperature can enhance the gasification of biochar and decomposition of macromolecular substances (Zhou et al., 2019), decreasing the biochar yield. At 750 °C, the highest pyrolytic liquid yield (36.6 wt%) was obtained.

The addition of attapulgite increased the yield of pyrolytic gas but decreased the yield of biochar and pyrolytic liquids. The yield of biochar, liquid and pyrolytic gas were 40.0 wt%, 34.3 wt% and 25.7 wt%, respectively, in the ratio of rWAS and attapulgite at 1:1 and temperature of 750 °C. The $Al_2O_3$ and $Fe_2O_3$ in attapulgite may promote the cracking reaction of organics in rWAS (Song et al., 2016; Yang et al., 2018). CaO and MgO can promote the reforming reaction of tar with $CO_2$ and $H_2O$, reducing the liquid yield while promoting the pyrolytic gas production (Zhou et al., 2014; Tang et al., 2018). Alkali metals ($Na_2O$, $K_2O$) in attapulgite may have affected the pyrolysis reactions, such as dehydroxylation and decarboxylation, increasing the non-condensable gases yield and reducing the biochar yield (Shimada et al., 2008).

### 3.3. Characteristics of liquid

The bio-oil and water in the pyrolytic liquid were clearly layered. With the catalysis of attapulgite, the $M$ value reduced and the O/C molar ratio of bio-oil decreased (Table 1). A high O content can negatively affect the fuel properties of bio-oil and may result in instability (Shen et al., 2016). The lowest $M$ value (12.8%) and O/C molar ratio (0.0265) of bio-oil was obtained at 1:1 of the ratio of rWAS to attapulgite and the termination temperature of 750 °C. $Al_2O_3$ in attapulgite promotes the deoxygenation reaction of O-containing compounds in vapor leading to more O element into non-condensable gases (Azuara et al., 2015).

The highest LHV (8.5 kcal/kg) of the bio-oil was detected at the rWAS:attapulgite of 1:0.75. The LHVs are related to the organic compositions. According to the GC-MS results, the organics in bio-oil can be divided into three groups: $<C_{13}$ (gasoline component), $C_{13}$–$C_{18}$ (diesel component) and $>C_{18}$ (heavy oil component) (Wang et al., 2007). The increase of attapulgite dosages significantly decreased the carbon numbers of organic compounds in bio-oil (Fig. 2b). When rWAS: attapulgite ratio at 1: 1, the content of $<C_{13}$ (28.7%) fraction in bio-oil doubled compared to without attapulgite addition (13.5%). Consequently, the content of $C_{13}$–$C_{18}$ fraction in bio-oil dramatically decreased. $Fe_2O_3$ in attapulgite may promote the generation of light fractions of bio-oil by enhancing the cracking reaction of C–C bonds in vapor during pyrolysis (Yang et al., 2018). At high temperature, the large molecules tend to break, resulting in the decrease of $C_{13}$–$C_{18}$ fraction. $Al_2O_3$ in attapulgite may further promote the polymerization of the $C_{12}$–$C_{18}$ fraction in

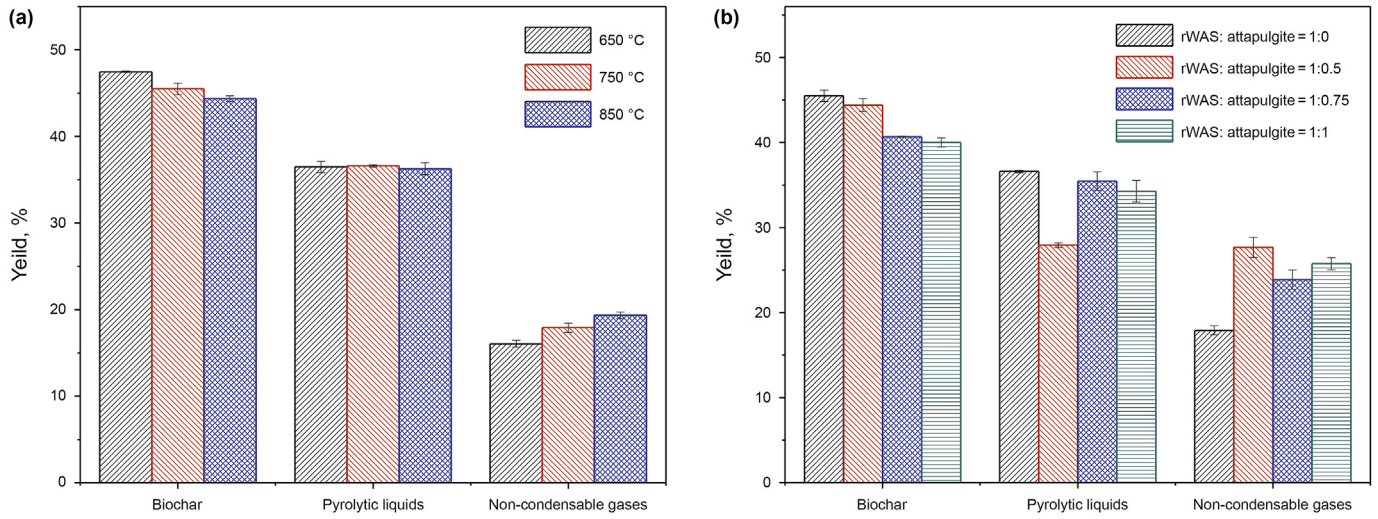


**Fig. 1.** Yields of products from pyrolysis of rWAS alone at different termination temperatures (a); yields of products from pyrolysis of rWAS under different rWAS: attapulgite ratios at termination temperature of 750 °C (b).

**Table 1**
Elemental compositions and LHVs of bio-oils resulting from different rWAS:attapulgite ratios.

| rWAS:attapulgite (mass ratios) | C | H | O | N | S | O/C | *M* (%) | LHV (kcal/kg) |
|---|---|---|---|---|---|---|---|---|
| 1:0 | 83.5 | 11.2 | 2.5 | 2.1 | 0.7 | 0.0304 | 14.6 | 6.8 |
| 1:0.5 | 84.1 | 11.2 | 2.5 | 2.1 | 0.8 | 0.0302 | 14.6 | 7.5 |
| 1:0.75 | 84.2 | 11.0 | 2.4 | 2.1 | 0.7 | 0.0285 | 13.8 | 8.5 |
| 1:1 | 84.0 | 10.9 | 2.2 | 2.1 | 0.8 | 0.0265 | 12.8 | 8.4 |

vapor, increasing the content of $>C_{18}$ heavy oil component (Azuara et al., 2015). Meanwhile, some newly generated small molecules may form aromatic substances, contributing to an increase of content of $<C_{13}$ fraction (Hu et al., 2018).

For bio-oil from pyrolysis of rWAS alone, the O-containing compounds (aldehydes, esters, alcohols and so on) dominated. The contents of aromatic hydrocarbons and alkanes were only 6.0% and 8.5%, respectively (Table 2). The attapulgite may promote the dehydroxylation and cracking reaction of acids and esters, increasing the content of alcohols and aldehydes (Fonts et al., 2012). Attapulgite mediated deoxygenation reaction may decrease the content of some O-containing compounds in bio-oil (Zhang et al., 2014). As shown in Table 2, there is not a clear trend with respect to all O-containing compounds. Some O-containing compounds may increase, and others will decrease.

The properties of bio-oil were further analyzed based on SARA results (Fig. 2c). The increase of attapulgite dosages significantly decrease the content of aromatics in bio-oil. $Fe_2O_3$ in attapulgite promotes the cracking of aromatic compounds in pyrolytic vapor (Yu et al., 2018). $Al_2O_3$ in attapulgite may further promote the formation of polycyclic compounds (Azuara et al., 2015). A low content of aromatics (10.2 wt%) and a high content of saturate (47.2 wt%) were obtained when the rWAS:attapulgite ratio was 1:1. Meanwhile, the content of resins and asphaltenes were very high and reached 42.6 wt% collectively. High temperature promotes the polymerization of polycyclic compounds and increases the content of resins and asphaltenes in bio-oils (Hu et al., 2018). The addition of attapulgite improved the bio-oil quality based on the higher content of light fraction, the low O mobility, as well as the lower O/C molar ratio.

### 3.4. Characteristics of pyrolytic gas

$CH_4$, $H_2$, CO and $CO_2$ are the main components in pyrolytic gas (Fig. 3). The aromatization reaction of alkanes in vapor may increase the $H_2$ content in pyrolytic gas. However, $Al_2O_3$ in attapulgite can crack oxygen functional groups derivatives to CO and $CO_2$ during the secondary decarboxylation reactions (Huo et al., 2018). Therefore, the total contents of CO and $CO_2$ increased, resulting in the decrease of $H_2$ content. The highest total content of $CO_2$ and CO reached 60.7 vol% and the lowest LHV of non-condensable gases was 3.1 kcal/$m^3$ when the rWAS:attapulgite ratio was set at 1:1. The non-condensable gases from pyrolysis of rWAS alone had the highest LHV (4.2 kcal/$m^3$) (Table S3).

$Fe_2O_3$ in attapulgite may intensify the cracking reaction of C–C bonds and reforming reaction of alkanes (Yang et al., 2018), increasing the $CH_4$ content (12.6 vol %) of non-condensable gases when the rWAS:attapulgite ratio was 1:0.5, compared to pyrolysis of rWAS alone (10.4 vol%). Further addition of attapulgite resulted in the production of less $CH_4$. This can be explained by the following. With the increase of attapulgite dosage, more $H_2O$ and $CO_2$ were released by dehydroxylation and decarboxylation (Fonts et al., 2012). The catalytic reforming reaction of steam may occur (Formulas 9, 10 and 11) (Mei et al. 2020). These reactions increase the content of $H_2$, CO and $CO_2$ in non-condensable gases. The highest content of $H_2$ (28.6 vol%) occurred at rWAS:attapulgite of 1:0.75. Alkali metal in attapulgite may reduce the generation of alkanes from rWAS and decrease the $CH_4$ content in non-condensable gases (Tang et al., 2018). Meanwhile, $CH_4$ may react with $CO_2$ and promote the formation of CO and $H_2$ (Formula 12) (Yu et al., 2018). The metal oxides in attapulgite can catalyze coke to

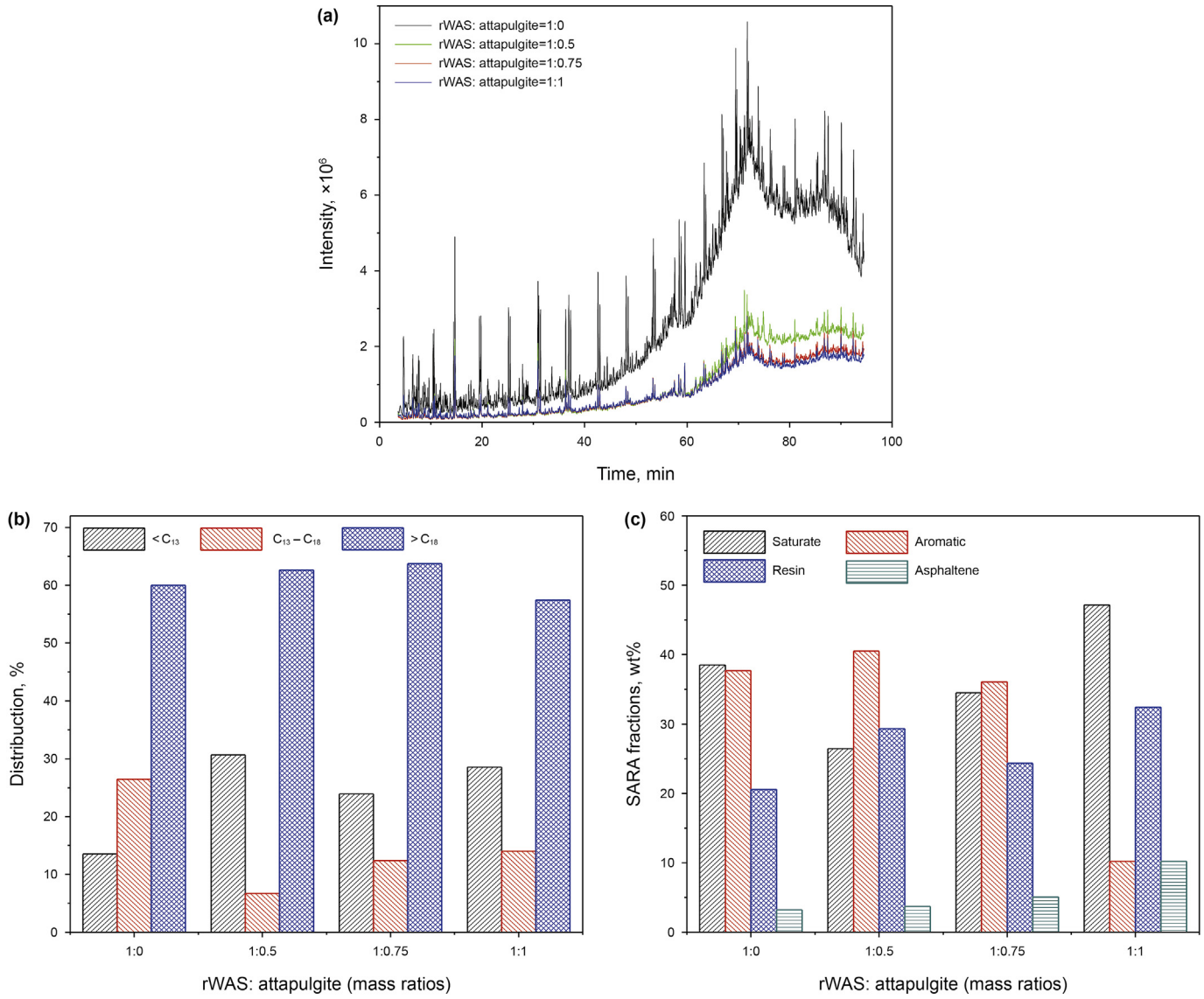


**Fig. 2.** Total ion chromatograms (a), carbon distribution (b), and SARA results (c) for bio-oils resulting from different rWAS: attapulgite ratios.

**Table 2**
Chemical compositions of bio-oils resulting from different rWAS:attapulgite ratios.

| rWAS:attapulgite (mass ratios) | 1:0 | 1:0.5 | 1:0.75 | 1:1 |
|---|---|---|---|---|
| Acids | 4.5 | 1.2 | 1.6 | 1.8 |
| Ketones | 1.2 | 2.4 | 2.6 | 2.1 |
| Aldehydes | 4.7 | 9.9 | 6.9 | 6.8 |
| Esters | 46.3 | 44.3 | 41.9 | 38.5 |
| Alkanes | 6.0 | 6.4 | 8.8 | 9.4 |
| Aromatics | 8.5 | 5.0 | 5.9 | 6.0 |
| Ethers | 1.6 | 1.4 | 1.3 | 1.7 |
| Alcohols | 21.7 | 19.5 | 24.1 | 27.6 |
| Others | 5.4 | 9.8 | 6.9 | 6.2 |
| Total content of O-containing compounds | 80.1 | 78.8 | 78.4 | 78.4 |

form CO and $CO_2$ (Formula 13) (Cheng et al., 2017).

High CO and $CO_2$ contents in pyrolytic gas are consistent with the low O/C molar ratio and *M* value in bio-oil. Therefore, attapulgite does not improve the quality of non-condensable gases according to the low LHV and content of $H_2$ and $CH_4$.

$$CH_4 + H_2O \rightarrow CO + 3H_2 \quad (9)$$

$$CO + H_2O \rightarrow H_2 + CO_2 \quad (10)$$

$$C + H_2O \rightarrow CO + H_2 \quad (11)$$

$$CH_4 + CO_2 \rightarrow 2CO + 2H_2 \quad (12)$$

$$M_xO_y + C/Coke \rightarrow M_xO_{y-1}/M + CO/CO_2 \quad (13)$$

### 3.5. Characteristics of pyrolytic residues

The attapulgite catalyzed pyrolysis significantly reduced the rWAS. The reduction rate of rWAS reached 60.0 wt% when the rWAS:attapulgite ratio was 1:1. Addition of attapulgite led to a higher reduction relative to rWAS alone (54.5 wt%). More biomass and oils in rWAS were converted to non-condensable gases and

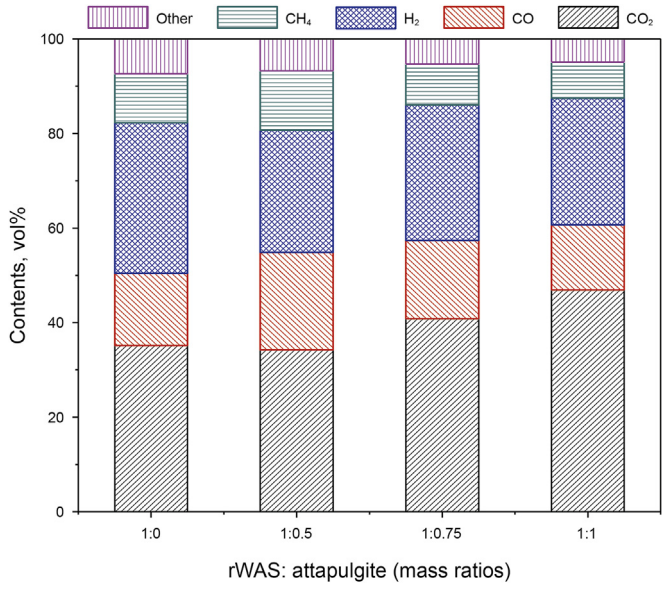


**Fig. 3.** Compositions of non-condensable gases resulting from different rWAS:attapulgite ratios.

bio-oil. Moreover, the attapulgite can hinder the coalescence of coke particles and promote the conversion of coke (Formula 11 and 13) (Bi et al., 2007). Less coke remained in the biochar, which resulted in the lowered LHV (1.1 kcal/kg) (Table 3).

The oils in rWAS were completely converted by pyrolysis. The oil content of residue is only 6.4 mg/kg when the ratio of rWAS to attapulgite was 1:1. The organics were converted to non-condensable gases, bio-oil, and biochar during high temperature catalytic pyrolysis. The content of residual state heavy metals in pyrolytic residues were higher than that of exchangeable state heavy metals (Table 3), showing the residue was relatively stable and with low toxicity to the environment (Zhai et al., 2014). The attapulgite addition decreased the contents of residual state Ni, Cr and Cu. Heavy metals in residual state have low biohazard and are relatively stable (Gao et al., 2020). With the increasing dosage of attapulgite, the contents of Co, Cr, Cu and Mn in residual state significantly increased. The attapulgite greatly promotes the immobilization of heavy metals when the rWAS:attapulgite ratio was 1:1, suggesting the low toxicity of pyrolytic residues (Xu et al., 2017). Overall, attapulgite catalyzed rWAS pyrolysis reduced environmental risks caused by organics and heavy metals. Exchangeable Mn in residue was mainly from attapulgite rather than rWAS. The addition of attapulgite likely increased the environmental risks of pyrolytic residue. The control of Mn release from attapulgite during pyrolysis should be investigated in future studies.

Typical adsorption peaks of C–H, O–H, C–O and C=O functional groups were detected in both of rWAS and pyrolytic residues, shown in Fig. 4 (Alvarez et al., 2016; Pentrák et al., 2018). C–H functional groups of hydrocarbons in FT-IR spectra generally include the aliphatic C–H stretching band (3100–2800 $cm^{-1}$), aromatic and olefinic C–H skeletal vibrations (1600–1700 $cm^{-1}$), aliphatic $-CH_2$ and $-CH_3$ deformation vibrations (1490–1365 $cm^{-1}$) and aliphatic C-$(CH_2)_n$-C (n = 1–3) rocking vibrations (700–900 $cm^{-1}$) (Gao et al., 2020). Compared to raw rWAS, the pyrolytic residue from rWAS alone showed low adsorption peaks of C–H stretching at 2960–2850 $cm^{-1}$ and C=O at 1520–1750 $cm^{-1}$, as well as a high adsorption peak of C–O stretching at 800–1210 $cm^{-1}$. Aliphatic chains, acids, and esters in raw rWAS are decomposed by pyrolysis and possibly converted to the alcohol, ethers and aldehydes (Song et al., 2016; Naqvi et al., 2019). The addition of attapulgite reduced the intensity of adsorption peaks of C–H deformation in the regions of 1500-1300 $cm^{-1}$and C–H stretching at 2960-2850 $cm^{-1}$ for the residue. Attapulgite may promote the breaking of aliphatic chains which may go on to form light hydrocarbons in the bio-oil, and it may also promote the production of $CH_4$ (Zhang et al., 2011). Adsorption peaks of C–O stretching found at 800-1210 $cm^{-1}$ and O–H stretching at 3459 $cm^{-1}$ significantly decreased by attapulgite addition. The attapulgite promotes deoxygenation, dehydroxylation and dehydrogenation reactions, producing more CO, $CO_2$ and $H_2O$ (Naqvi et al., 2019). The $H_2O$ may participate in the reforming reaction (Formula 9, 10 and 11), increasing CO and $CO_2$ in non-condensable gases and reducing the O/C of bio-oil.

### 3.6. Catalytic pyrolysis mechanism of attapulgite

The catalytic pyrolysis of rWAS with different dosages of attapulgite occurs in three stages from TG and DTG curves (Fig. 5). Stage I (230–400 °C) corresponds to the decomposition and reforming reaction of light components (Naqvi et al., 2019). Stage II (400–500 °C) is mainly related to the decomposition of bacterial matter (e.g. protein and polysaccharide) and some macromolecular aliphatic compounds (Liu et al., 2015; Prashanth et al., 2021). The decomposition and devolatilization of light char both contribute to a small weight loss that occurs in Stage III (620–720 °C) (Dai et al., 2015). The decomposition of rWAS mainly occurred during Stage I and II. The addition of attapulgite significantly promoted the weight loss of rWAS relative to rWAS alone.

The pyrolysis of rWAS and attapulgite aided rWAS both followed the second-order reaction kinetics (Fig. S1, Table 4). The addition of attapulgite significantly decreased the *E* values of Stage I and II in comparison with sewage sludge (82.3 kJ/mol and 48.3 kJ/mol) (Gao et al., 2014). Compared to rWAS alone, the *E* values decreased from 21.7 kJ/mol to 13.8 kJ/mol and 46.9 kJ/mol to 23.6 kJ/mol in Stage I and II, respectively, for rWAS:attapulgite ratio of 1:1. The *E* value of Stage III, however, increased with the addition of attapulgite. The decomposition and devolatilization of light char may require a higher temperature (Liu et al., 2015). The pre-exponential factor (*A*) increased with the increase of termination temperature and the addition of attapulgite. Usually, the value of *A* reflects the effective contact between reactant molecules in a reaction. Therefore, a high

**Table 3**
Exchangeable state (F1) and residual state (F5) of heavy metals in attapulgite and pyrolytic residues.

| rWAS: attapulgite (mass ratios) | F1 (mg/kg) | | | | | F5 (mg/kg) | | | | |
|---|---|---|---|---|---|---|---|---|---|---|
| | Co | Ni | Cr | Cu | Mn | Co | Ni | Cr | Cu | Mn |
| attapulgite | – | – | – | 0.1 | – | 1.60 | 13.6 | 19.9 | 19.9 | 354.5 |
| 1:0 | – | – | – | 0.1 | 3.4 | – | 231.9 | 55.9 | 55.9 | 150.6 |
| 1:0.5 | – | – | – | 0.1 | 13.1 | 2.10 | 109.7 | 28.7 | 28.7 | 226.3 |
| 1:0.75 | – | – | – | – | 10.0 | 1.40 | 82.9 | 26.0 | 26.0 | 264.9 |
| 1:1 | – | – | – | – | 7.7 | 4.25 | 108.4 | 39.3 | 39.3 | 405.8 |

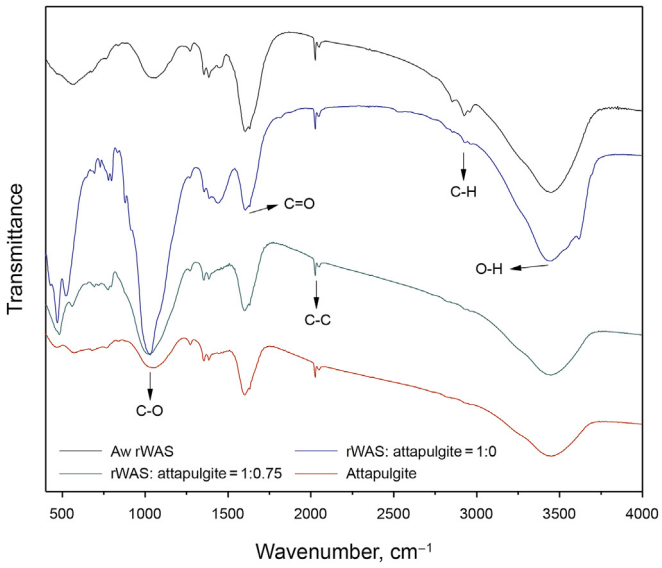


**Fig. 4.** FTIR spectra of raw rWAS, attapulgite and pyrolytic residues.

value of *A* indicates that the reaction rate of organic matter in rWAS is promoted by attapulgite during the thermal decomposition reaction (Gao et al., 2014).

The catalytic effects of attapulgite on rWAS mainly act on enhancing the devolatilization of rWAS in Stage I and the reformation of primary vapors in Stage II (Fig. 6) (Lin et al., 2019). Attapulgite also promotes the decomposition of remaining heavy organic matter, such as bacterial matter and some macromolecular aliphatic compounds, reducing the yield of biochar. The secondary decomposition of the pyrolytic vapor was further catalyzed by $Fe_2O_3$ in attapulgite and rWAS, increasing the content of $<C_{13}$ components (Yang et al., 2018). The dehydrogenation, dehydroxylation and deoxygenation reactions of the pyrolytic vapor were also catalyzed by metallic oxides to release $H_2O$, $CO_2$ and CO (Zhang et al., 2014; Ozbay et al., 2019). This results in the increased content of alcohols and aldehydes, while decreased the O mobility towards bio-oil. Steam ($H_2O$) aided reforming reactions increase the content of $H_2$, CO and $CO_2$ in non-condensable gases (Formula 9, 10, 11 and 12). The metallic oxides in attapulgite may react with coke, reducing the amount of biochar and producing CO and $CO_2$ at high temperature in Stage III (Formula 13) (Cheng et al., 2017).

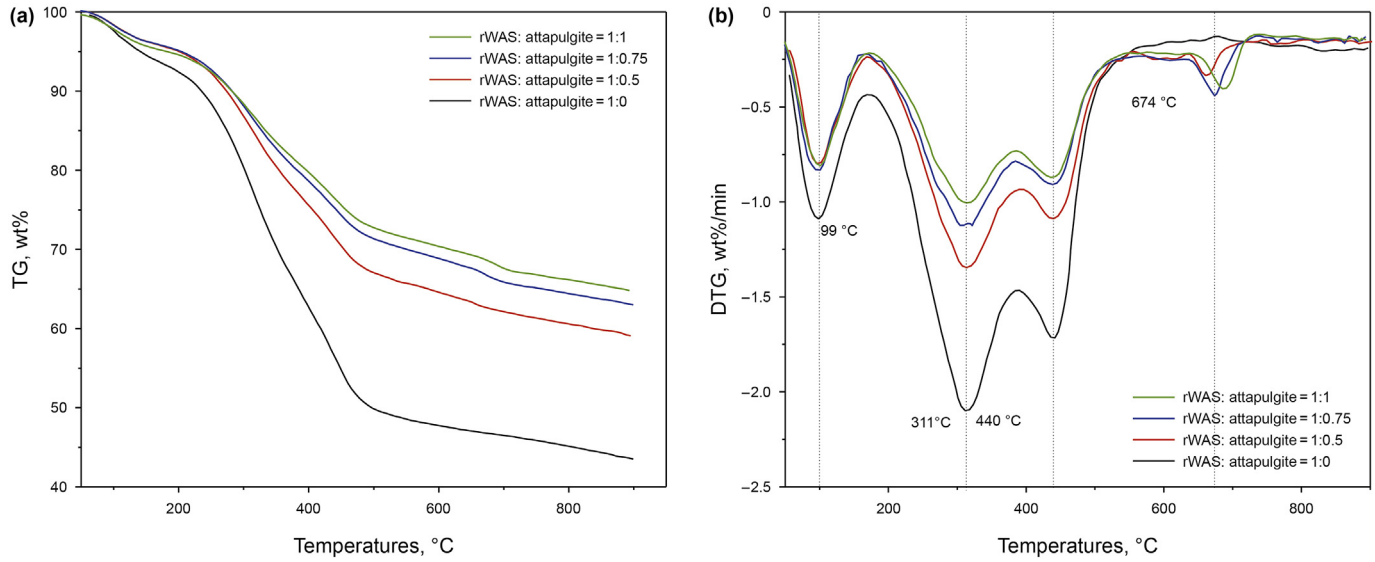


**Fig. 5.** TG (a) and DTG (b) curves of rWAS with different dosages of attapulgite.

**Table 4**
Pyrolysis dynamic parameters of rWAS with different dosages of attapulgite.

| rWAS: attapulgite (mass ratios) | Stage (°C) | Fitting equations | $R^2$ | *E* (kJ/mol) | *A* ($min^{-1}$) |
|---|---|---|---|---|---|
| 1:0 | 233–403 | y = −2605.3x-7.4689 | 0.9914 | 21.7 | 1.49E+01 |
| | 403–498 | y = −5644.1x-3.0167 | 0.9895 | 46.9 | 2.76E+03 |
| 1:0.5 | 230–397 | y = −2127.6x-8.4104 | 0.9909 | 17.7 | 4.73E+00 |
| | 397–496 | y = −3394.6x-6.5634 | 0.9904 | 28.2 | 4.79E+01 |
| | 604–711 | y = −3833.8x-6.6319 | 0.9879 | 31.9 | 6.56E+01 |
| 1:0.75 | 238–395 | y = −1872.8x-8.8559 | 0.9922 | 15.6 | 2.67E+00 |
| | 395–496 | y = −2728.7x-7.6211 | 0.9909 | 22.7 | 4.01E+01 |
| | 642–724 | y = −6754.4x-3.6956 | 0.9884 | 56.2 | 1.68E+03 |
| 1:1 | 244–402 | y = −1655.4x-9.2178 | 0.9939 | 13.8 | 1.64E+00 |
| | 402–498 | y = −2840.9x-7.4837 | 0.9909 | 23.6 | 1.60E+01 |
| | 650–725 | y = −8068.9x-2.3833 | 0.9842 | 67.1 | 7.44E+03 |

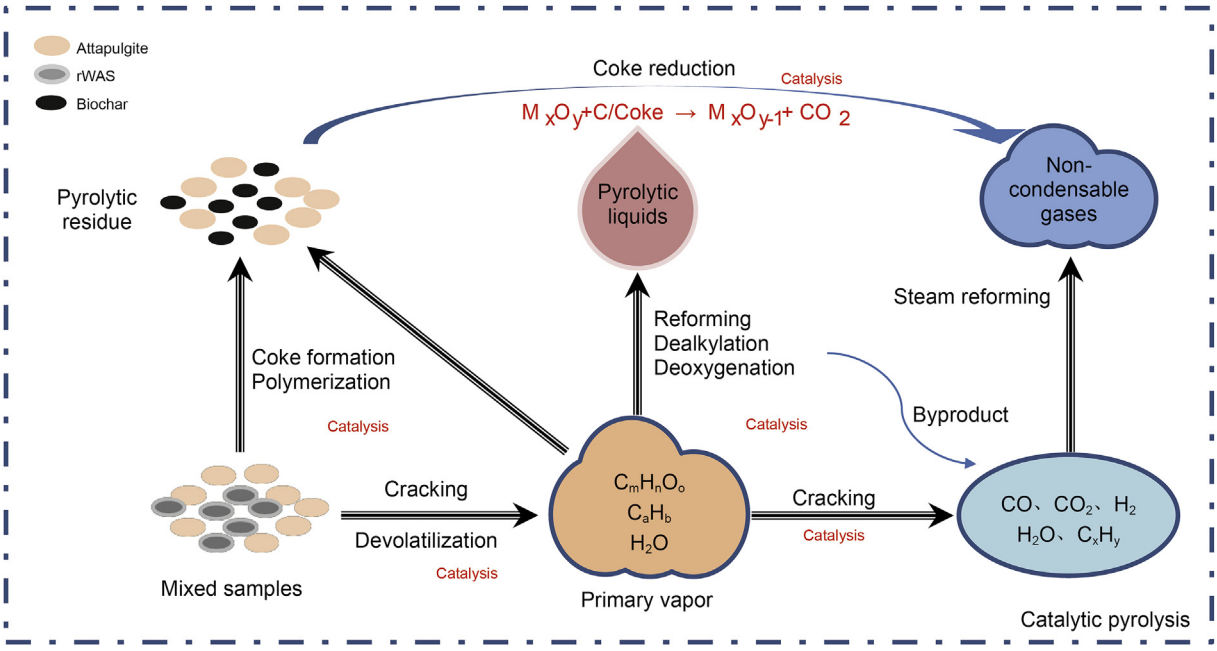


**Fig. 6.** Proposed reaction process of attapulgite catalyzed pyrolysis of rWAS.

## 4. Conclusions

Attapulgite decreased the activation energy of rWAS pyrolysis, reduced the biochar production and enhanced the quality of bio-oil. The metallic oxides in attapulgite promoted a series of catalytically thermal reactions of biomass and oils, including cracking, dehydrogenation, dehydroxylation and deoxygenation. Compared to rWAS alone, attapulgite catalyzed pyrolysis increased LHVs, the contents of $<C_{13}$ fractions and saturates, decreased the O mobility and the O/C molar ratio in bio-oil, and reduced the environmental risks caused by organics and heavy metals in pyrolytic residue. This research showed the potential application of natural attapulgite in the catalytic pyrolysis of rWAS.

## Acknowledgments

This study was supported by National Key R&D Program of China (2018YFC1801903-01 and 2019YFC1806201-01), National Natural Science Foundation of China (No. 21776307), and Science Foundation of China University of Petroleum-Beijing (No. 2462018BJB001 and 2462020YXZZ035).

## Appendix A. Supplementary data

Supplementary data to this article can be found online at https://doi.org/10.1016/j.petsci.2021.09.043.

## Conflicts of interest

The authors declare no conflict of interest.

## References

Alvarez, J., Lopez, G., Amutio, M., Artetxe, M., Barbarias, I., Arregi, A., Bilbao, J., Olazar, M., 2016. Characterization of the bio-oil obtained by fast pyrolysis of sewage sludge in a conical spouted bed reactor. Fuel Process. Technol. 149, 169–175. https://doi.org/10.1016/j.fuproc.2016.04.015.

Azuara, M., Fonts, I., Bimbela, F., Murillo, M.B., Gea, G., 2015. Catalytic post-treatment of the vapors from sewage sludge pyrolysis by means of $\gamma$-$Al_2O_3$: effect on the liquid product properties. Fuel Process. Technol. 130, 252–262. https://doi.org/10.1016/j.fuproc.2014.10.014.

Bi, W.D., McCaffrey, W.C., Gray, M.R., 2007. Agglomeration and deposition of coke during cracking of petroleum vacuum residue. Energy Fuel. 21, 1205–1211. https://doi.org/10.1021/ef0602630.

Cheng, S., Wang, Y.H., Fumitake, T., Kouji, T., Li, A., Kunio, Y., 2017. Effect of steam and oil sludge ash additive on the products of oil sludge pyrolysis. Appl. Energy 185, 146–157. https://doi.org/10.1016/j.apenergy.2016.10.055.

Cui, H., Qian, Y., Li, Q., Wei, Z.B., Zhai, J.P., 2013. Fast removal of Hg(II) ions from aqueous solution by amine-modified attapulgite. Appl. Clay Sci. 72, 84–90. https://doi.org/10.1016/j.clay.2013.01.003.

Dai, Q.J., Jiang, X.G., Lv, G.J., Ma, X.J., Jin, Y.Q., Wang, F., Chi, Y., Yan, J.H., 2015. Investigation into particle size influence on PAH formation during dry sewage sludge pyrolysis: TG-FTIR analysis and batch scale research. J. Anal. Appl. Pyrol. 112, 388–393. https://doi.org/10.1016/j.jaap.2014.09.015.

Fonts, I., Gea, G., Azuara, M., Ábrego, J., Arauzo, J., 2012. Sewage sludge pyrolysis for liquid production: a review. Renew. Sustain. Energy Rev. 16, 2781–2805. https://doi.org/10.1016/j.rser.2012.02.070.

Gao, N.B., Li, J.J., Qi, B.Y., Li, A.M., Duan, Y., Wang, Z., 2014. Thermal analysis and products distribution of dried sewage sludge pyrolysis. J. Anal. Appl. Pyrol. 105, 43–48. https://doi.org/10.1016/j.jaap.2013.10.002.

Gao, N.B., Li, J.Q., Quan, C., Tan, H.Z., 2020. Product property and environmental risk assessment of heavy metals during pyrolysis of oily sludge with fly ash additive. Fuel 266, 117090. https://doi.org/10.1016/j.fuel.2020.117090.

Gil-Lalaguna, N., Sánchez, J.L., Murillo, M.B., Ruiz, V., Gea, G., 2014. Air-steam gasification of char derived from sewage sludge pyrolysis. Comparison with the gasification of sewage sludge. Fuel 129, 147–155. https://doi.org/10.1016/j.fuel.2014.03.059.

Gong, Z.Q., Wang, Z.T., Wang, Z.B., 2018. Study on migration characteristics of heavy metals during oil sludge incineration. Petrol. Sci. Technol. 36, 469–474. https://doi.org/10.1080/10916466.2018.1430156.

Han, R., Zhao, C.X., Liu, J.W., Chen, A.X., Wang, H.T., 2015. Thermal characterization and syngas production from the pyrolysis of biophysical dried and traditional thermal dried sewage sludge. Bioresour. Technol. 198, 276–283. https://doi.org/10.1016/j.biortech.2015.08.071.

Hu, S., Han, H.D., Syed-Hassan, S.S.A., Zhang, Y.N., Wang, Y., Zhang, L.P., He, L.M., Su, S., Jiang, L., Cheng, J.F., Xiang, J., 2018. Evolution of heavy components during sewage sludge pyrolysis: a study using an electrospray ionization Fourier transform ion cyclotron resonance mass spectrometry. Fuel Process. Technol. 175, 97–103. https://doi.org/10.1016/j.fuproc.2018.03.036.

Huo, X.D., Xiao, J., Song, M., Zhu, L., 2018. Comparison between in-situ and ex-situ catalytic pyrolysis of sawdust for gas production. J. Anal. Appl. Pyrol. 135, 189–198. https://doi.org/10.1016/j.jaap.2018.09.003.

Karaca, C., Sözen, S., Orhon, D., Okutan, H., 2018. High temperature pyrolysis of sewage sludge as a sustainable process for energy recovery. Waste Manag. 78, 217–226. https://doi.org/10.1016/j.wasman.2018.05.034.

Li, X., Zong, Z.M., Ma, W.W., Wei, Z.H., Li, Y., Cao, J.P., Mayyas, M., Li, Z.K., Wei, X.Y., 2015. A highly active Ni/mesoporous attapulgite for hydrocracking CO bonds in rice straw. Fuel Process. Technol. 131, 376–381. https://doi.org/10.1016/j.fuproc.2014.12.007.

Lin, B.C., Huang, Q.X., Ali, M., Wang, F., Chi, Y., Yan, J.H., 2019. Continuous catalytic

pyrolysis of oily sludge using U-shape reactor for producing saturates-enriched light oil. Proc. Combust. Inst. 37, 3101–3108. https://doi.org/10.1016/j.proci.2018.05.143.
Lin, B.C., Wang, J., Huang, Q.X., Chi, Y., 2017. Effects of potassium hydroxide on the catalytic pyrolysis of oily sludge for high-quality oil product. Fuel 200, 124–133. https://doi.org/10.1016/j.fuel.2017.03.065.
Liu, G.R., Song, H.J., Wu, J.H., 2015. Thermogravimetric study and kinetic analysis of dried industrial sludge pyrolysis. Waste Manag. 41, 128–133. https://doi.org/10.1016/j.wasman.2015.03.042.
Liu, H.B., Chen, T.H., Zhang, X.L., Li, J.H., Chang, D.Y., Song, L., 2010. Effect of additives on catalytic cracking of biomass gasification tar over a nickel-based catalyst. Chin. J. Catal. 31, 409–414. https://doi.org/10.1016/S1872-2067(09)60061-9.
Liu, J.G., Jiang, X.M., Zhou, L.S., Wang, H., Han, X.X., 2009. Co-firing of oil sludge with coal–water slurry in an industrial internal circulating fluidized bed boiler. J. Hazard Mater. 167, 817–823. https://doi.org/10.1016/j.jhazmat.2009.01.061.
Mishra, H., Karmakar, S., Kumar, R., Singh, J., 2017. A framework for assessing uncertainty associated with human health risks from MSW landfill leachate contamination. Risk Anal. 37, 1237–1255. https://doi.org/10.1111/risa.12713.
Naqvi, S.R., Tariq, R., Hameed, Z., Ali, I., Naqvi, M., Chen, W.H., Ceylan, S., Rashid, H., Ahmad, J., Taqvi, S.A., Shahbaz, M., 2019. Pyrolysis of high ash sewage sludge: kinetics and thermodynamic analysis using Coats-Redfern method. Renew. Energy 131, 854–860. https://doi.org/10.1016/j.renene.2018.07.094.
Nges, I.A., Liu, J., 2010. Effects of solid retention time on anaerobic digestion of dewatered-sewage sludge in mesophilic and thermophilic conditions. Renew. Energy 35, 2200–2206. https://doi.org/10.1016/j.renene.2010.02.022.
Ozbay, N., Yargic, A.S., Sahin, R.Z.Y., Yaman, E., 2019. Valorization of banana peel waste via in-situ catalytic pyrolysis using Al-Modified SBA-15. Renew. Energy 140, 633–646. https://doi.org/10.1016/j.renene.2019.03.071.
Pentrák, M., Hronský, V., Pálková, H., Uhlík, P., Komadel, P., Madejová, J., 2018. Alteration of fine fraction of bentonite from Kopernica (Slovakia) under acid treatment: a combined XRD, FTIR, MAS NMR and AES study. Appl. Clay Sci. 163, 204–213. https://doi.org/10.1016/j.clay.2018.07.028.
Prashanth, P.F., Burada, S., Vinu, R., Lavanya, M., Prabu, V.R., 2021. Production of diesel range hydrocarbons from crude oil sludge via microwave-assisted pyrolysis and catalytic upgradation. Process Saf Environ 146, 383–395. https://doi.org/10.1016/j.psep.2020.08.025.
Raheem, A., Sikarwar, V.S., He, J., Dastyar, W., Dionysiou, D.D., Wang, W., Zhao, M., 2018. Opportunities and challenges in sustainable treatment and resource reuse of sewage sludge: a review. Chem. Eng. J. 337, 616–641. https://doi.org/10.1016/j.cej.2017.12.149.
Shao, J.G., Yan, R., Chen, H.P., Yang, H.P., Lee, D.H., 2010. Catalytic effect of metal oxides on pyrolysis of sewage sludge. Fuel Process. Technol. 91, 1113–1118. https://doi.org/10.1016/j.fuproc.2010.03.023.
Shen, Y.F., Chen, X.M., Wang, J.F., Ge, X.L., Chen, M.D., 2016. Oil sludge recycling by ash-catalyzed pyrolysis-reforming processes. Fuel 182, 871–878. https://doi.org/10.1016/j.fuel.2016.05.102.
Shen, Y.F., Yoshikawa, K., 2013. Recent progresses in catalytic tar elimination during biomass gasification or pyrolysis-A review. Renew. Sustain. Energy Rev. 21, 371–392. https://doi.org/10.1016/j.rser.2012.12.062.
Shimada, N., Kawamoto, H., Saka, S., 2008. Different action of alkali/alkaline earth metal chlorides on cellulose pyrolysis. J Anal Pyrol 81, 80–87. https://doi.org/10.1016/j.jaap.2007.09.005.
Song, J., Yang, J.K., Liang, S., Shi, Y.F., Yu, W.B., Li, C., Xu, X.Y., Xiao, J., Guan, R.N., Ye, N., Wu, X., Hou, H.J., Hu, J.P., Hu, J.K., Xiao, B., 2016. Red mud enhanced hydrogen production from pyrolysis of deep-dewatered sludge cakes conditioned with Fenton's reagent and red mud. Int. J. Hydrogen Energy 41, 16762–16771. https://doi.org/10.1016/j.ijhydene.2016.06.217.
Syed-Hassan, S.S.A., Wang, Y., Hu, S., Su, S., Xiang, J., 2017. Thermochemical processing of sewage sludge to energy and fuel: fundamentals, challenges and considerations. Renew. Sustain. Energy Rev. 80, 888–913. https://doi.org/10.1016/j.rser.2017.05.262.
Tang, S.Q., Zheng, C.M., Yan, F., Shao, N.N., Tang, Y.Y., Zhang, Z.T., 2018. Product characteristics and kinetics of sewage sludge pyrolysis driven by alkaline earth metals. Energy 153, 921–932. https://doi.org/10.1016/j.energy.2018.04.108.
Wang, Z.Q., Guo, Q.J., Liu, X.M., Cao, C.Q., 2007. Low temperature pyrolysis characteristics of oil sludge under various heating conditions. Energy Fuel. 21, 957–962. https://doi.org/10.1021/ef060628g.
Xu, Q.Y., Tang, S.Q., Wang, J.C., Ko, J.H., 2017. Pyrolysis kinetics of sewage sludge and its biochar characteristics. Process Saf Environ 115, 49–56. https://doi.org/10.1016/j.psep.2017.10.014.
Yang, G., Zhang, G.M., Wang, H.C., 2015. Current state of sludge production, management, treatment and disposal in China. Water Res. 78, 60–73. https://doi.org/10.1016/j.watres.2015.04.002.
Yang, J.K., Xu, X.Y., Liang, S., Guan, R.N., Li, H.S., Chen, Y., Liu, B.C., Song, J., Yu, W.B., Xiao, K.K., Hou, H.J., Hu, J.P., Yao, H., Xiao, B., 2018. Enhanced hydrogen production in catalytic pyrolysis of sewage sludge by red mud: thermogravimetric kinetic analysis and pyrolysis characteristics. Int. J. Hydrogen Energy 43, 7795–7807. https://doi.org/10.1016/j.ijhydene.2018.03.018.
Ye, H.F., Liu, B.D., Wang, Q.H., How, Z.T., Zhan, Y.L., Chelme-Ayala, P., Guo, S.H., Ei-Din, M.G., Chen, C.M., 2020. Comprehensive chemical analysis and characterization of heavy oil electric desalting wastewaters in petroleum refineries. Sci. Total Environ. 724, 138117. https://doi.org/10.1016/j.scitotenv.2020.138117.
Yu, G.T., Chen, D.Z., Arena, U., Huang, Z., Dai, X.H., 2018. Reforming sewage sludge pyrolysis volatile with Fe-embedded char: minimization of liquid product yield. Waste Manag. 73, 464–475. https://doi.org/10.1016/j.wasman.2017.08.004.
Zabłocka-Malicka, M., Szczepaniak, W., Zielińska, A., Rutkowski, P., 2016. Steam gasification of oat with conversion of tars on clay catalyst and gas cleaning by condensation of steam. Ecol Chem Eng S 23, 33–48. https://doi.org/10.1515/eces-2016-0002.
Zhai, Y.B., Chen, H.M., Xu, B.B., Xiang, B.B., Chen, Z., Li, C.T., Zeng, G.M., 2014. Influence of sewage sludge-based activated carbon and temperature on the liquefaction of sewage sludge: yield and composition of bio-oil, immobilization and risk assessment of heavy metals. Bioresour. Technol. 159, 72–79. https://doi.org/10.1016/j.biortech.2014.02.049.
Zhang, B.P., Xiong, S.J., Xiao, B., Yu, D.K., Jia, X.Y., 2011. Mechanism of wet sewage sludge pyrolysis in a tubular furnace[J]. Int. J. Hydrogen Energy 36, 355–363. https://doi.org/10.1016/j.ijhydene.2010.05.100.
Zhang, X.D., Sun, L.Z., Chen, L., Xie, X.P., Zhao, B.F., Si, H.Y., Meng, G.F., 2014. Comparison of catalytic upgrading of biomass fast pyrolysis vapors over CaO and Fe(III)/CaO catalysts. J. Anal. Appl. Pyrol. 108, 35–40. https://doi.org/10.1016/j.jaap.2014.05.020.
Zhao, X.B., Meng, Y.Q., Lu, X.W., Li, X.Z., 2013. Sol–gel synthesis and catalytic property of $Ce_{1-x}Ti_xO_2$ nanocomposites supported on attapulgite clay. J. Sol. Gel Sci. Technol. 66, 22–30.
Zhou, C.G., Stuermer, T., Gunarathne, R., Yang, W.H., Blasiak, W., 2014. Effect of calcium oxide on high-temperature steam gasification of municipal solid waste. Fuel 122, 36–46. https://doi.org/10.1016/j.fuel.2014.01.029.
Zhou, Y., Liu, Y.Z., Jiang, W.B., Shao, L.L., Zhang, L.Q., Feng, L., 2019. Effects of pyrolysis temperature and addition proportions of corncob on the distribution of products and potential energy recovery during the preparation of sludge activated carbon. Chemosphere 221, 175–183. https://doi.org/10.1016/j.chemosphere.2019.01.026.